Role of alkali ions in the near-zero thermal expansion of NaSICON-type $AZr_2(PO_4)_3$ (A = Na, K, Rb, Cs) and $Zr_2(PO_4)_3$ compounds

Xi Zhen,[1] Andrea Sanson,[2,3] Qiang Sun,[1,*] Erjun Liang,[1] and Qilong Gao[1,†]

[1]*Key Laboratory of Materials Physics of Ministry of Education, and School of Physics and Microelectronics, Zhengzhou University, Zhengzhou 450052, China*

[2]*Department of Physics and Astronomy, University of Padua, Padova I-35131, Italy*

[3]*Department of Management and Engineering, University of Padua, Padova I-35131, Italy*

(Received 23 April 2023; revised 11 September 2023; accepted 21 September 2023; published 10 October 2023)

Zero thermal expansion (ZTE) is a rare phenomenon of great importance in the field of materials design. $AZr_2(PO_4)_3$ (A = Na, K, Rb, Cs) exhibit near-zero thermal expansion. In this work, we perform first principles calculations in $AZr_2(PO_4)_3$ (A = Na, K, Rb, Cs) and $Zr_2(PO_4)_3$ compounds to elucidate the effects of A cations on the thermal expansion behavior. Structural and vibrational analysis shows that the near-zero thermal expansion is strongly related to the dynamics of the "lantern" units of $[Zr_2(PO_4)_3]$, where the ZrO_6 and PO_4 polyhedra are rigid. The calculated Grüneisen parameters reveal that different A-site alkali metal atoms heavily affect the phonon modes of A atoms and the rotation of ZrO_6 and PO_4 polyhedra, as well as the acoustic phonon modes, thus resulting in a different thermal expansion behavior of $AZr_2(PO_4)_3$ (A = Na, K, Rb, Cs). The absence of A atoms in $Zr_2(PO_4)_3$ facilitates the structural flexibility and therefore the occurrence of a stronger negative thermal expansion. This work provides insights into the modulation of thermal expansion of these $NaZr_2(PO_4)_3$-type compounds.

DOI: 10.1103/PhysRevB.108.144102

I. INTRODUCTION

Zero thermal expansion (ZTE, i.e., volume remains constant within a certain temperature range) is a rare and interesting phenomenon [1]. Due to their excellent dimensional stability, ZTE materials are important for materials design, such as in high-precision applications. Some examples of single-phase near ZTE materials are $Zn_4B_6O_{13}$, which exhibits a solid cagelike structure, and the coupled rotation of BO_4 tetrahedra with the Zn-O bond constraint leads to ZTE [2,3], and $Ta_2Mo_2O_{11}$ where the positive thermal expansion (PTE) intralayers are balanced by negative thermal expansion (NTE) interlayers thus resulting in overall ZTE [4]. Very interesting is the case of nano ScF_3, whose ZTE originates from the suppression of transverse vibrations of F atoms [5]. Other typical ZTE materials are TaO_2F [6], $ZrMgMo_3O_{12}$ [7], $MgZrF_6$ [8], $Fe[Co(CN)_6]$ [9], and $Sc_{1.5}Al_{0.5}W_3O_{12}$ [10]. However, the number of ZTE materials is low and not sufficient to satisfy the application needs. With the discovery of NTE phenomenon (shrink upon heating) [11–13], the opportunity to regulate the thermal expansion of materials has become feasible. In principle, ZTE materials can be obtained by compounding NTE and PTE materials, just like $Mn_3Cu_{0.5}Ge_{0.5}N/Cu$ or ZrO_2/ZrW_2O_8 [14,15].

Chemical substitution is a common way to regulate the thermal expansion of materials. For example, with the change of M and A atoms in $MZrF_6$ (M = Ca, Mn, Fe, Co, Ni, Zn) and $A_2O(PO_4)_2$ (A = Th, U, Zr), the thermal expansion can be modulated from NTE to PTE [16,17]. In $Ni_2P_2O_7$, replacing Ni with different ratios of Mn, we can regulate the phase transition temperature and broaden the NTE temperature region. In particular, $Ni_{1.4}Mn_{0.6}P_2O_7$ exhibits near ZTE in the temperature range 180–420 K [18]. In framework structures, the introduction of guest species is also an effective way to control thermal expansion. For instance, ZTE can be obtained by insertion of Na^+ ions and H_2O molecules in $GaFe(CN)_6$ and $TiCo(CN)_6$, respectively, thanks to the inhibition of the transverse vibrations of CN bridge atoms [19,20]. Also the transition from NTE to ZTE to PTE in ScF_3 is achieved by adjusting the amount of inserted Li^+ ions which suppresses the transverse vibrations of F atoms [21]. In general, either chemical substitution or introduction of guest species affect crystal structure flexibility, chemical bonds, atomic vibrations, and magnetic and electronic properties, and thus can modulate the thermal expansion behavior of materials.

$NaZr_2(PO_4)_3$ type compounds (NZP) are of wide interest for their negative or low thermal expansion coefficient, fast ionic conductivity, tunable anisotropic thermal expansion, facile ionic substitution, and thermal stability [22–24]. The chemical formula of NZP can be expressed as $M1M2L_2(TO_4)_3$. Two LO_6 octahedra and three TO_4 tetrahedra form the so-called "lantern" unit of $[L_2(TO_4)_3]$, which are aligned along the c axis and form holes in the crystal structure. There are two types of hole locations, related to $M1$ and $M2$ cations, where the $M1$ site can be replaced by alkali metal ions and the $M2$ site, in most cases, is unoccupied [25]. NZP materials generally exhibit anisotropic thermal expansion with

*qsun@zzu.edu.cn
†qilonggao@zzu.edu.cn

positive expansion in the c axis and negative expansion in the a (b) axis [26]. Taking $NaZr_2(PO_4)_3$ as an example, where the Na ions occupy only the $M1$ sites, Alamo argued that the expansion of the Na-O bonds contributes significantly to the thermal expansion of NZP materials: the Na-O bonds expand and the space in the $M1$ sites along the c axis increases, thus causing the expansion of the crystallographic c axis and the coupled rotations of the ZrO_6 octahedra and PO_4 tetrahedra connected by shared angles, thus creating the conditions to have NTE along the a (b) axis [27]. Moreover, it was shown that the thermal expansion of the NZP family is heavily influenced by the cations at the M site. For example, in $Na_{1-x}Nb_xZr_{2-x}(PO_4)_3$, $Na_{1+x}Zr_2(Si_xP_{3-x})O_{12}$, and $Na_{1+x}Y_xZr_{2-x}(PO_4)_3$, for $0 \leqslant x \leqslant 1$, the Na ions occupy only the $M1$ sites, and as the Na content increases, the c axis and its thermal expansion increase significantly. When $x > 1$, the $M1$ sites are fully occupied (except for $Na_{1+x}Zr_2(Si_xP_{3-x})O_{12}$) and $M2$ sites start to be occupied. As the Na content increases, the a axis and its thermal expansion coefficient increase. However, in this case, the thermal expansion caused by the occupation of the $M2$ sites leads to the contraction of the PO_4 tetrahedra, resulting in a low thermal expansion of the a (b) axis [28]. In particular, when the M sites are not occupied by ions, such as $TaTi(PO_4)_3$ and $NbTi(PO_4)_3$, more free spaces in the crystal structure lead to a more flexible structure, which facilitates rotational motion between the polyhedra and the occurrence of negative thermal expansion behavior [29,30].

It is also important to point out that the M-site ionic radius influences the thermal expansion. For example, in the $MHf_2(PO_4)_3$ series, where M = Na, K, Rb, Cs, when the M site is occupied by a large ion, the O-P-O bond angle expands in the c axis and the bridging PO_4 tetrahedra contract along the a-axis direction, promoting a decrease of the average thermal expansion [31]. The M site can also be occupied by a two-valent cation, such as $M_{0.5}Zr_2(PO_4)_3$ (M = Ca, Sr, Ba). In this family, to balance the valence, only one M atom is included in each primitive cell. The positive thermal expansion of $M_{0.5}Zr_2(PO_4)_3$ (M = Ca, Sr, Ba) gradually increases as the radius of M^{2+} increases and $BaZr_2(PO_4)_3$ exhibits a different thermal expansion behavior than most NZP compounds: $\alpha_c < 0$ and α_a, $\alpha_b > 0$ [32,33]. For the $AZr_2(PO_4)_3$ (A = Na, K, Rb, Cs) family, the $M1$ sites are completely occupied by A cations and the average thermal expansion coefficient α_{av} [$\alpha_{av} = (\alpha_a + \alpha_b + \alpha_c)/3$] of $NaZr_2(PO_4)_3$, $KZr_2(PO_4)_3$, $RbZr_2(PO_4)_3$, $CsZr_2(PO_4)_3$ is 4.5×10^{-6} K^{-1}, -0.4×10^{-6} K^{-1}, -0.36×10^{-6} K^{-1}, 0.4×10^{-6} K^{-1} in the temperature range 293–1273 K, respectively [34,35]. The thermal expansion of $AZr_2(PO_4)_3$ (A = Na, K, Rb, Cs) changes irregularly as the radius of the A-site cation increases ($Na^+ < K^+ < Rb^+ < Cs^+$). So far, it is not clear how the A-site cation affects the thermal expansion behavior of the $AZr_2(PO_4)_3$ family.

In this work, to clarify the different effect of A cations in the thermal expansion of the $AZr_2(PO_4)_3$ family, first-principles calculations have been performed for the cases A = Na, K, Rb, Cs and in the absence of A atoms. The structural and dynamic properties were investigated to reveal the factors that promote the occurrence of near-zero thermal expansion. By comparing the differences in Grüneisen parameters, the influence of the various A atoms on specific phonon modes and thus on the different thermal expansion behavior of $AZr_2(PO_4)_3$ compounds has been clarified.

II. COMPUTATIONAL DETAILS

All calculations were carried out within the context of density functional theory (DFT) by using the Vienna Ab initio Simulation Package (VASP) [36]. The ion-electron interaction was described using the projector augmented wave (PAW) function approach. The exchange and correlation effects were included within the Perdew-Burke-Ernzerhof (PBE) generalized gradient approximation (GGA) [37]. The wave functions for the primitive cell of $AZr_2(PO_4)_3$ (A = Na, K, Rb, Cs) and $Zr_2(PO_4)_3$ are expanded by plane waves up to an energy cutoff of 600 eV. The integration over the Brillouin zone is sampled with a k-point grid of $4 \times 4 \times 4$, generated automatically by the Monkhorst-Pack approach [38]. The convergence criteria for the total energy and ionic forces were set to 10^{-8} eV and 10^{-4} eV/Å, respectively.

In order to obtain the phonon properties by the PHONOPY code [39], we have picked a $2 \times 2 \times 2$ supercell with $2 \times 2 \times 2$ k-point mesh and used the finite displacement method developed in VASP to calculate the force constants [40]. The thermodynamic properties have been calculated within the quasiharmonic approximation (QHA) [41]. The QHA theory contains only implicit anharmonicity (i.e., the volume dependence of phonon frequencies) and ignores explicit anharmonicity (i.e., phonon-phonon anharmonic interactions, which may contribute significantly at high temperature) [42,43]. Therefore, this approach has been widely used to calculate the thermal expansion properties of materials well below their melting points [44–49]. The Helmholtz free energy versus volume ($F-V$) for ten different volumes around the optimized equilibrium volume has been fitted by the Vinet equation of states (EOS) [50] in order to obtain the thermal expansion coefficient (CTE). The mode Grüneisen parameters have been calculated according to the definition $\gamma_{q,j} = -\frac{V}{\omega_{q,j}}\frac{\partial \omega_{q,j}}{\partial V}$ [51].

III. RESULTS AND DISCUSSION

A. Crystal structure and thermal expansion properties

The crystal structure of trigonal $AZr_2(PO_4)_3$ (A = Na, K, Rb, Cs) with space group $R\bar{3}C$ is shown in Fig. 1(a): two ZrO_6 octahedra are connected by three PO_4 tetrahedra to form a "lantern" unit of $[Zr_2(PO_4)_3]$ [for clarity, Fig. 1(b) shows two neighboring lantern units], with the A-site alkali metal atom located between the two lantern units along the c axis. The structure of $AZr_2(PO_4)_3$ (A = Na, K, Rb, Cs) has been optimized and the calculated lattice constants and bond lengths are in good agreement with the experimental values [52,53] as reported in Table I. In particular, it can be observed that the a axis gradually decreases and the c axis gradually increases as the radius of the A-site cation increases ($Na^+ < K^+ < Rb^+ < Cs^+$). We have also simulated the crystal structure without A atoms [i.e., $Zr_2(PO_4)_3$, not successfully synthesized experimentally], and the optimized crystal structure is basically unchanged as shown in Fig. 1(c). The calculated phonon spectra without imaginary frequencies (see below for detailed information) prove that the structure is stable.

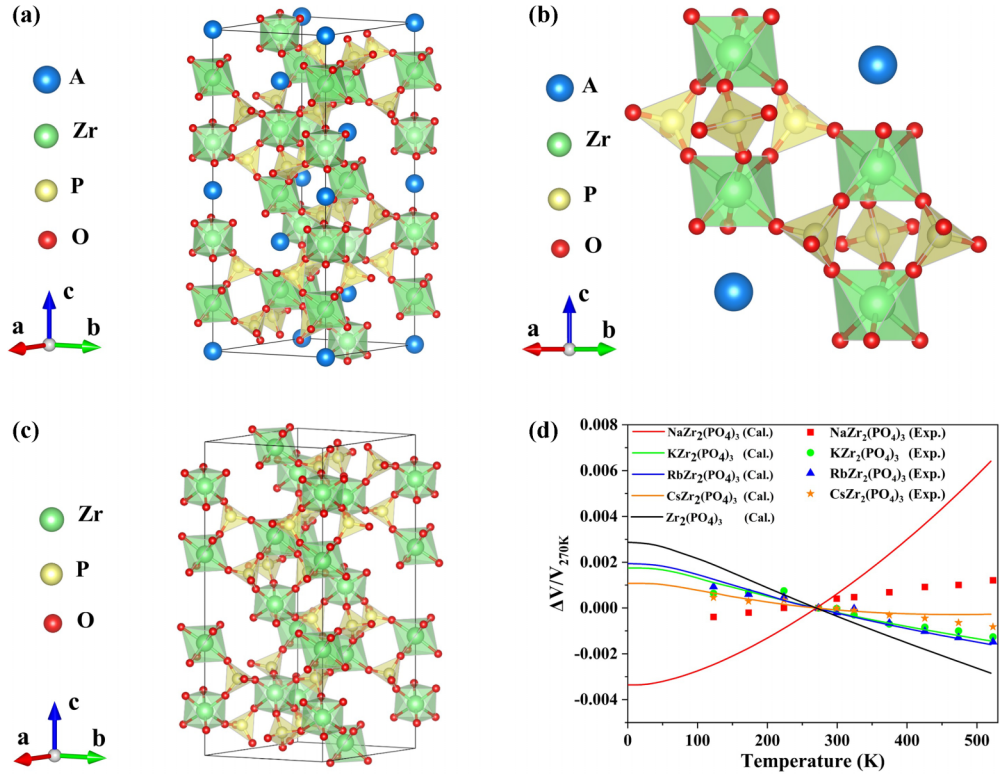

FIG. 1. (a) Crystal structure of $AZr_2(PO_4)_3$ (A = Na, K, Rb, Cs); (b) two neighboring lantern units of $[Zr_2(PO_4)_3]$; (c) crystal structure of $Zr_2(PO_4)_3$; (d) calculated (lines) and experimental (symbols) [54] relative thermal expansion of $AZr_2(PO_4)_3$ and $Zr_2(PO_4)_3$.

The relative volume thermal expansion of $AZr_2(PO_4)_3$ (A = Na, K, Rb, Cs) and $Zr_2(PO_4)_3$ has been calculated in the temperature range 0–520 K and compared with the experimental data [54], as shown in Fig. 1(d). The calculated linear CTE (approximated as $\alpha_l = \frac{\alpha_V}{3}$) and experimental average CTE are listed in Table II. The calculated values are fully consistent with the experimental data, except for the overestimation of the PTE of $NaZr_2(PO_4)_3$. Indeed, in the low temperature region 0–520 K, the PTE of $NaZr_2(PO_4)_3$, the NTE of $KZr_2(PO_4)_3$ and $RbZr_2(PO_4)_3$, and the lower NTE of $CsZr_2(PO_4)_3$ have been reproduced. Finally, Table II also reports the calculated elastic constants and bulk modulus, whose results are similar to those calculated by Kamali *et al.* [55].

The calculated charge densities (Fig. 2) indicate that all Zr-O and P-O bonds exhibit covalent bonding properties, resulting in rigid ZrO_6 and PO_4 polyhedra (in particular the PO_4 tetrahedra will be highly rigid due to the short P-O bonds and the localized charge density). When the A element changes, the Zr-O and P-O bond lengths and charge density distributions are very similar, demonstrating that the different A element does not affect the Zr-O and P-O bond properties much. Thus, the lantern unit $[Zr_2(PO_4)_3]$ formed by the rigid ZrO_6 and PO_4 polyhedra is very solid and facilitates the near-zero thermal expansion behavior of $AZr_2(PO_4)_3$ (A = Na, K, Rb, Cs).

B. Phonon properties

The thermal expansion of materials with framework structures is closely related to phonon properties. The phonon dispersion curves and the density of vibrational states of these five compounds are shown in Fig. 3. $AZr_2(PO_4)_3$ (A = Na, K,

TABLE I. Calculated and experimental [52,53] lattice constants and bond lengths in $AZr_2(PO_4)_3$ (A = Na, K, Rb, Cs) and $Zr_2(PO_4)_3$.

	$NaZr_2(PO_4)_3$		$KZr_2(PO_4)_3$		$RbZr_2(PO_4)_3$		$CsZr_2(PO_4)_3$		$Zr_2(PO_4)_3$	
	Calc.	Expt.	Calc.	Expt.	Calc.	Expt.	Calc.	Expt.	Calc.	Expt.
a (Å)	8.91	8.80	8.84	8.73	8.78	8.71	8.71	8.58	9.01	
b (Å)	8.91	8.80	8.84	8.73	8.78	8.71	8.71	8.58	9.01	
c (Å)	22.91	22.76	24.13	23.97	24.63	24.3	25.15	24.9	23.08	
V (Å^3)	1576	1527	1633	1580	1644	1596	1651	1586	1621	
Zr-O1 (Å)	2.11	2.08	2.10	2.10	2.10	2.11	2.09	2.16	2.07	
Zr-O2 (Å)	2.06	2.04	2.08	2.06	2.08	2.07	2.09	2.0	2.09	
P-O1 (Å)	1.55	1.55	1.55	1.54	1.55	1.53	1.55	1.54	1.54	
P-O2 (Å)	1.54	1.53	1.54	1.57	1.54	1.58	1.54	1.54	1.54	

TABLE II. Calculated elastic constants, bulk modulus, and calculated linear CTEs (α_l) and experimental average CTE (α_{av}) [54] in $AZr_2(PO_4)_3$ (A = Na, K, Rb, Cs) and $Zr_2(PO_4)_3$ compounds.

	$NaZr_2(PO_4)_3$	$KZr_2(PO_4)_3$	$RbZr_2(PO_4)_3$	$CsZr_2(PO_4)_3$	$Zr_2(PO_4)_3$
C_{11}	128.465	178.117	196.881	211.437	112.642
C_{12}	51.881	73.431	72.938	69.15	63.191
C_{13}	61.320	87.296	87.541	83.443	76.796
C_{14}	-12.739	-17.77	-18.716	-17.675	-17.437
C_{33}	161.994	164.246	154.301	146.025	155.201
C_{44}	53.247	53.214	53.136	52.457	41.688
C_{66}	46.537	47.169	49.426	53.922	32.194
B (GPa)	87.760	113.522	111.347	105.335	85.624
Calc. α_l ($\times 10^{-6}$ K^{-1})	6.4	-2.1	-2.4	-0.8	-3.9
Expt. α_{av} ($\times 10^{-6}$ K^{-1})	1.4	-1.9	-2.1	-1.1	

Rb, Cs) present similar phonon spectra [see Figs. 3(a)–3(d)], which can be divided in three regions: low frequency (0–12.5 THz), middle frequency (15–20 THz), and high frequency (27.5–35 THz). It can be observed that the vibrations of the A-site alkali metal atoms are mainly located in the ultralow frequency region, and the vibrational contribution becomes more concentrated at lower frequencies as the mass of the A atom increases. Also, the vibrations of the Zr atoms occur mainly in the low frequency region, with a weak contribution in the middle frequency region. The P and O atoms contribute in the whole frequency region, with a stronger contribution from O atoms. An interesting aspect, Fig. 3(e) indicates that the frequencies of all phonon modes in $Zr_2(PO_4)_3$ are lowered compare to $AZr_2(PO_4)_3$ compounds, and the density of states of Zr, P, and O atoms is similar to that of $AZr_2(PO_4)_3$.

We have analyzed the eigenvectors of all phonon modes at the Γ point of the Brillouin zone and calculated the corresponding square displacements ($u_j^2 = \frac{|e_j|^2}{m_j}$) [56] of the different types of atoms to investigate the vibrational motion, as shown in Fig. 4. $AZr_2(PO_4)_3$ (A = Na, K, Rb, Cs) and $Zr_2(PO_4)_3$ exhibit similar vibrational properties. The phonon modes in the frequency range 0–8 THz correspond to coupled rotations (RUM) and bending motions of ZrO_6 and PO_4 polyhedra (mainly contributing to NTE), vibrations of A atoms, and translational motions of PO_4 polyhedra and Zr atoms. In the frequency range 8–19 THz, the phonon modes mainly contribute to PTE and are associated to the bending of Zr-O2-P and Zr-O1-P bonds and motions of P atoms. The phonon modes from 28–35 THz all contribute to the PTE and are associated to the stretching motion of the P-O bonds.

C. Effect of *A*-site alkali metal atoms on the thermal expansion

In quasiharmonic approximation the contribution of the different phonon modes to the thermal expansion depends on the positive or negative value of the corresponding mode Grüneisen parameter: the larger the negative value of the mode Grüneisen parameter, the stronger the contribution to the NTE. In $AZr_2(PO_4)_3$ and $Zr_2(PO_4)_3$ compounds, all phonon modes are in the middle and high frequency region with low positive values of Grüneisen parameter which will not contribute to the anomalous thermal expansion, so we focus on the mode Grüneisen parameter in the low frequency region as shown in Fig. 5. It is clear that the phonon modes of $KZr_2(PO_4)_3$, $RbZr_2(PO_4)_3$, and $Zr_2(PO_4)_3$ with negative Grüneisen parameters dominate from 0 to 11 THz [see Figs. 5(b), 5(c), and 5(e)], corresponding to the NTE behavior of these three compounds from 0 to 520 K. Interestingly, the three acoustic phonon branches also contribute to the NTE. In comparison, the phonon modes of $CsZr_2(PO_4)_3$ contribute less to the NTE in the low frequency region [see Fig. 5(d)], for example, the negative mode Grüneisen parameters are weakened and the acoustic modes contribute mainly to the PTE, leading to a very weak NTE. In $NaZr_2(PO_4)_3$, the phonon

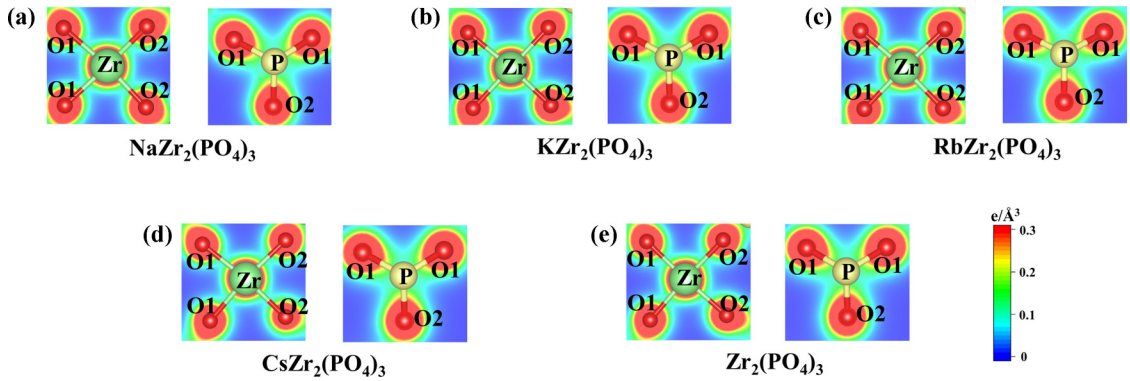

FIG. 2. Calculated charge density of (a) $NaZr_2(PO_4)_3$, (b) $KZr_2(PO_4)_3$, (c) $RbZr_2(PO_4)_3$, (d) $CsZr_2(PO_4)_3$, and (e) $Zr_2(PO_4)_3$.

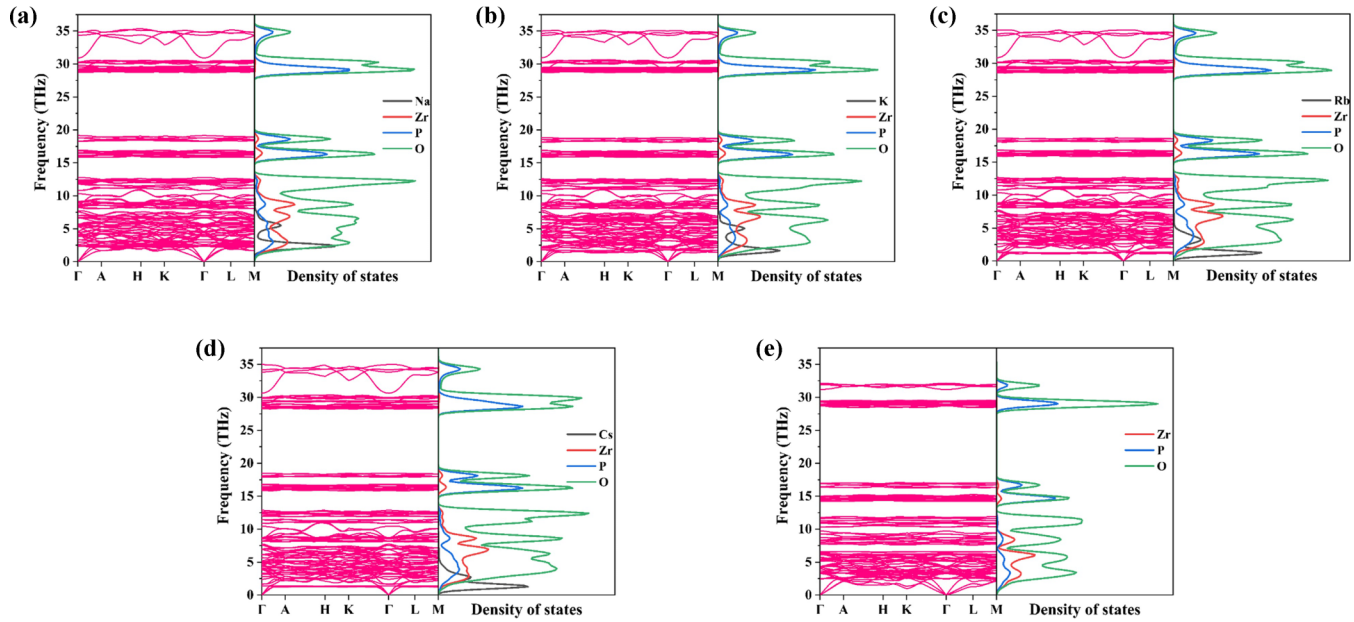

FIG. 3. Calculated phonon dispersion curves and phonon density of states for (a) $NaZr_2(PO_4)_3$, (b) $KZr_2(PO_4)_3$, (c) $RbZr_2(PO_4)_3$, (d) $CsZr_2(PO_4)_3$, and (e) $Zr_2(PO_4)_3$.

modes that contribute to the PTE dominate from 0 to 11THz [see Fig. 5(a)], consistent with its PTE nature.

To obtain more detailed information, we have extracted the Grüneisen parameters of all phonon modes within a $30 \times 30 \times 30$ grid in the Brillouin zone and processed them into point density maps for the low frequency region (0–8 THz), as shown in Fig. 6. Figure 6(a) shows that a large number of optical phonon modes of $NaZr_2(PO_4)_3$ near 2.4 THz have a positive Grüneisen parameter and so contribute significantly to the PTE, and these vibrational modes involve the motion of Na atoms. Differently, in $KZr_2(PO_4)_3$ and $RbZr_2(PO_4)_3$, the phonon modes where K and Rb play a dominant role [see Figs. 6(b) and 6(c), at about 1.7 and 1.5 THz, respectively] have negative Grüneisen parameters and therefore contribute to NTE. Figure 6(d) shows that the phonon modes related to Cs atoms near 1.3 THz contribute weakly to the PTE.

The eigenvectors of the phonon mode of $AZr_2(PO_4)_3$ (A = Na, K, Rb, Cs) in which the A atom plays a dominant role at the Γ point (the E_u mode as an example) are shown in Fig. 7(a). In addition, the phonon modes in $AZr_2(PO_4)_3$ and $Zr_2(PO_4)_3$ that contribute most to the NTE are the rotational coupling motion of ZrO_6 and PO_4 polyhedron, which are

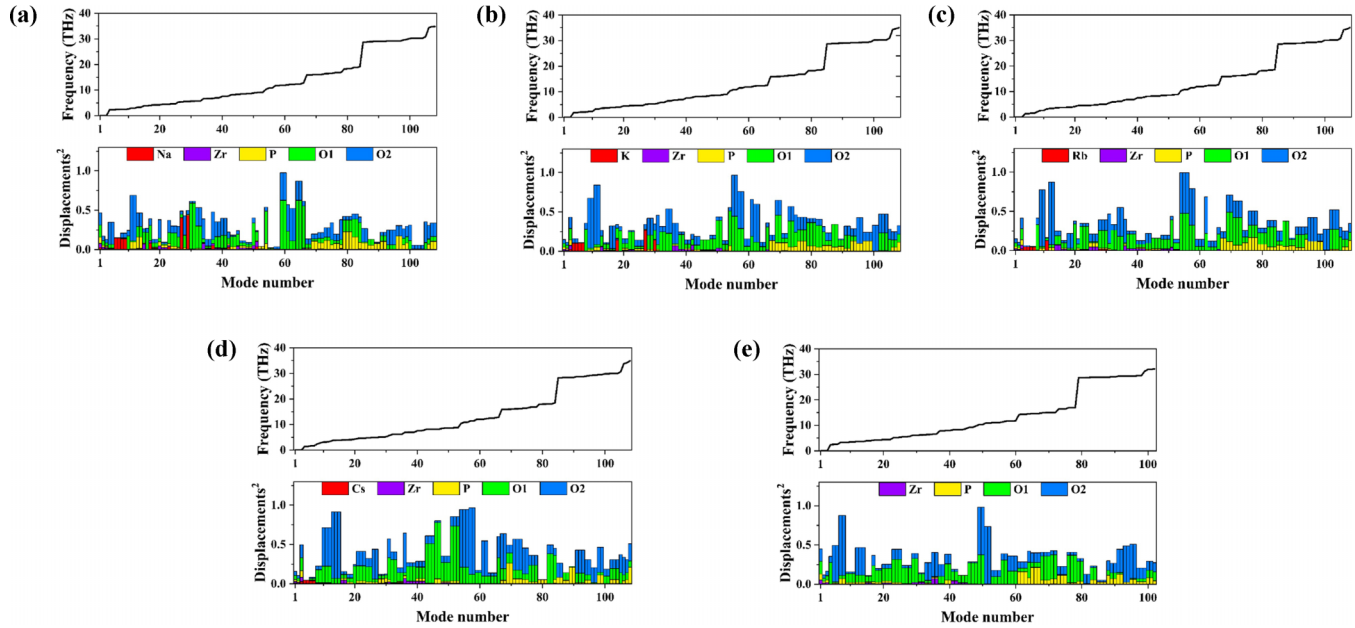

FIG. 4. Calculated phonon frequency (top panels) and square displacements (bottom panels) of each atom type for all phonon modes at Γ points in (a) $NaZr_2(PO_4)_3$, (b) $KZr_2(PO_4)_3$, (c) $RbZr_2(PO_4)_3$, (d) $CsZr_2(PO_4)_3$, and (e) $Zr_2(PO_4)_3$. The results are normalized to 1.

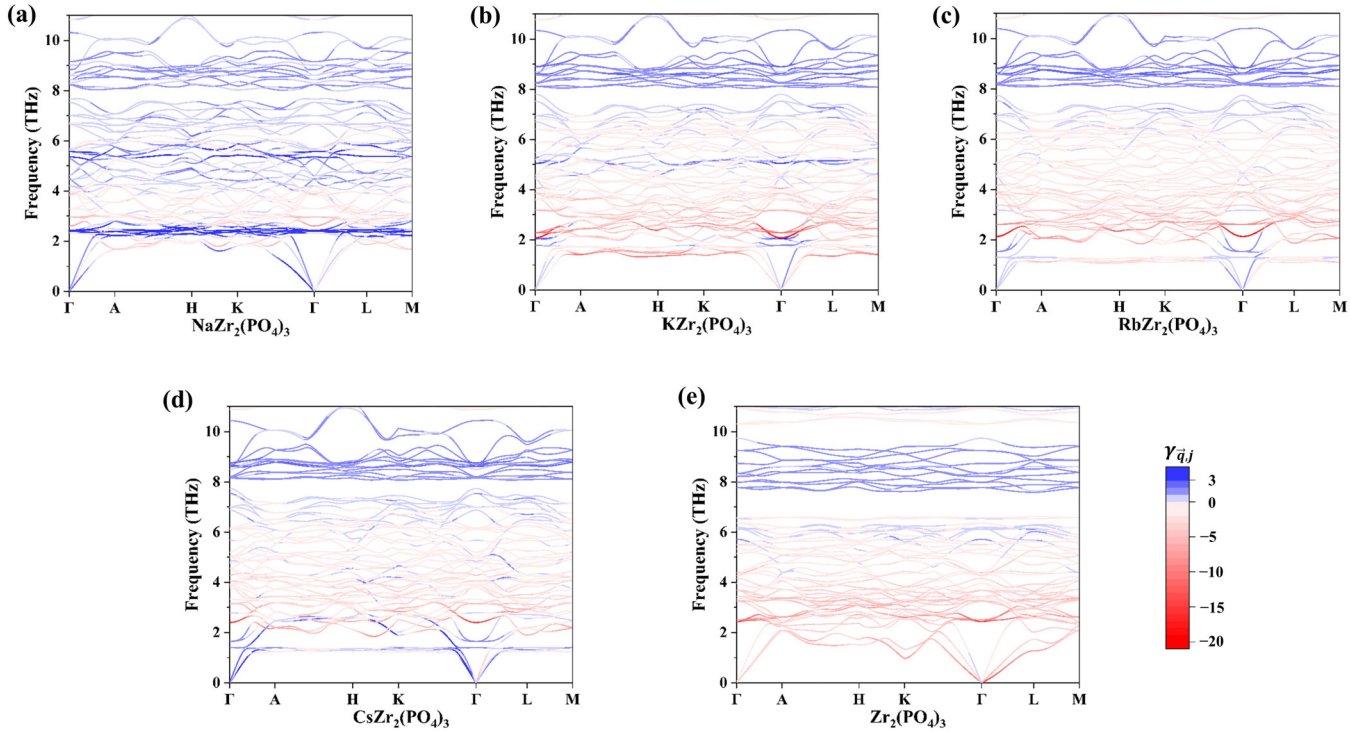

FIG. 5. Calculated low frequency phonon dispersion curves of (a) $NaZr_2(PO_4)_3$, (b) $KZr_2(PO_4)_3$, (c) $RbZr_2(PO_4)_3$, (d) $CsZr_2(PO_4)_3$, and (e) $Zr_2(PO_4)_3$. The colored scale ranges from blue for positive Grüneisen parameters, to red for negative Grüneisen parameters.

RUM and give rise to the contraction along the a and b axes; the eigenvectors of this vibrational mode (the A_{2g} mode at the Γ point as an example) are shown in Fig. 7(b). The Grüneisen parameters of these two representative modes are also listed in Table III. From Figs. 6(b) and 6(c), it is clear that the coupled rotational modes in $KZr_2(PO_4)_3$ and $RbZr_2(PO_4)_3$ (at about

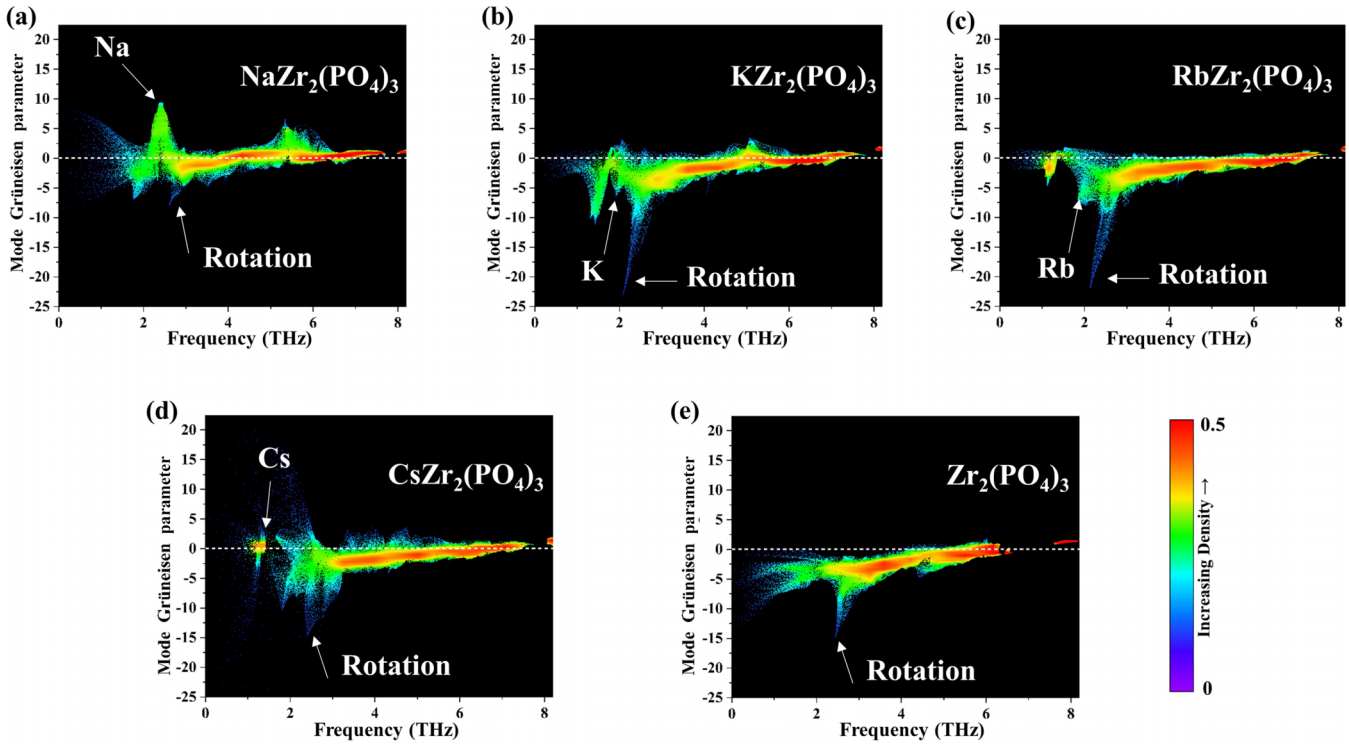

FIG. 6. The point density map of mode Grüneisen parameters in (a) $NaZr_2(PO_4)_3$, (b) $KZr_2(PO_4)_3$, (c) $RbZr_2(PO_4)_3$, (d) $CsZr_2(PO_4)_3$, and (e) $Zr_2(PO_4)_3$ in the low frequency range 0–8 THz.

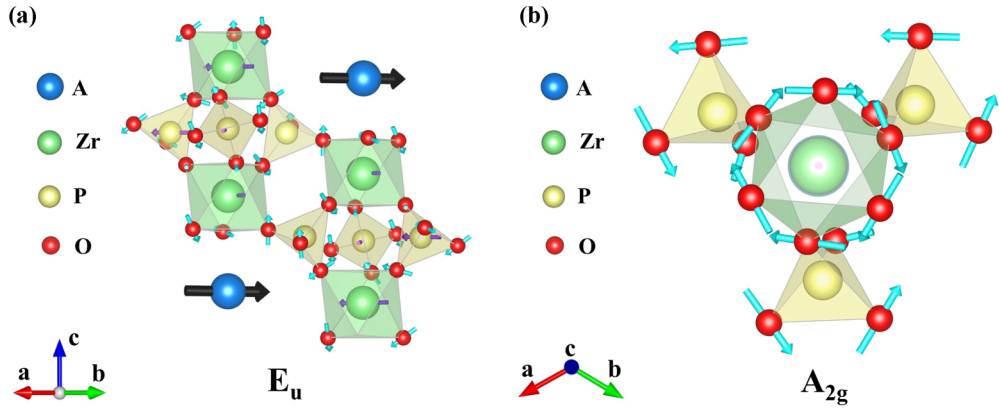

FIG. 7. Eigenvectors of the E_u and A_{2g} modes in $AZr_2(PO_4)_3$ (A = Na, K, Rb, Cs) and $Zr_2(PO_4)_3$.

2.1 THz) have the largest negative Grüneisen parameters and contribute the most to the NTE. In contrast, the coupled rotational modes in $CsZr_2(PO_4)_3$ [see Fig. 6(d), at around 2.4 THz] contribute less to NTE and that of $NaZr_2(PO_4)_3$ [see Fig. 6(a), around 2.6 THz] even less. To summarize the above analysis, when the A-site alkali metal ion changed, the contribution of specific three phonon models [(1) the mode dominated by A-site alkali metal ions; (2) RUM, i.e., rotation modes of ZrO_6 octahedron and PO_4 tetrahedron; (3) acoustic phonon modes] to the NTE followed the order $KZr_2(PO_4)_3 \approx RbZr_2(PO_4)_3 > CsZr_2(PO_4)_3 > NaZr_2(PO_4)_3$, resulting in $KZr_2(PO_4)_3$ and $RbZr_2(PO_4)_3$ exhibiting similar low NTE properties, $CsZr_2(PO_4)_3$ exhibiting very weak NTE properties, and $NaZr_2(PO_4)_3$ exhibiting low PTE properties. In addition, Figs. 5(e) and 6(e) show that the number of phonon modes with negative Grüneisen parameter are higher when the A-site alkali metal ion is not present [i.e., $Zr_2(PO_4)_3$]. The frequency of all phonon modes in $Zr_2(PO_4)_3$ were decreased [see Fig. 3(e)], resulting in easier excitation of phonon modes which contribute to NTE, thus $Zr_2(PO_4)_3$ exhibits relatively strong NTE properties.

Finally, to evaluate the overall thermal expansion, we have calculated the overall Grüneisen parameter $\bar{\gamma}$ which represents the weighted sum of all phonon modes excited at a certain temperature. Figure 8 shows that the calculated $\bar{\gamma}$ is consistent with the thermal expansion behavior of the five compounds here investigated: $\bar{\gamma}$ is negative in $KZr_2(PO_4)_3$, $RbZr_2(PO_4)_3$, $CsZr_2(PO_4)_3$, and $Zr_2(PO_4)_3$, and positive in $NaZr_2(PO_4)_3$. In particular, $CsZr_2(PO_4)_3$ exhibits the smallest negative value of $\bar{\gamma}$, in accordance with its smallest NTE, while $KZr_2(PO_4)_3$ and $RbZr_2(PO_4)_3$ show a similar negative value of $\bar{\gamma}$, consistent with their similar low NTE. Finally, $Zr_2(PO_4)_3$ shows the most negative value of $\bar{\gamma}$ indicating the largest NTE, and $NaZr_2(PO_4)_3$ exhibits a positive $\bar{\gamma}$ in agreement with its PTE behavior.

TABLE III. Grüneisen parameters of the E_u and A_{2g} modes in $AZr_2(PO_4)_3$ (A = Na, K, Rb, Cs) and $Zr_2(PO_4)_3$.

	E_u		A_{2g}	
	ω (THz)	$\gamma_{q,j}$	ω (THz)	$\gamma_{q,j}$
$NaZr_2(PO_4)_3$	2.4	9.5	2.6	-7.8
$KZr_2(PO_4)_3$	1.8	1.5	2.1	-23.1
$RbZr_2(PO_4)_3$	1.3	1.0	2.1	-21.9
$CsZr_2(PO_4)_3$	1.4	1.3	2.4	-14.7
$Zr_2(PO_4)_3$			2.4	-14.8

IV. CONCLUSIONS

In summary, $AZr_2(PO_4)_3$ (A = Na, K, Rb, Cs) and $Zr_2(PO_4)_3$ compounds have been investigated by first principles calculations to clarify their different low thermal expansion behavior and the effect of the A-site alkali metal atoms on the thermal expansion. The calculated charge density indicates that all Zr-O and P-O bonds are covalent, resulting in a rigid ZrO_6 octahedra and PO_4 tetrahedra of the $[Zr_2(PO_4)_3]$ lantern units. This is an important aspect which can be related to the presence of the low thermal expansion behavior. The vibrational analysis shows that the phonon modes in the low frequency region (0–8 THz) mainly contribute to the negative thermal expansion, in particular the coupled rotational modes

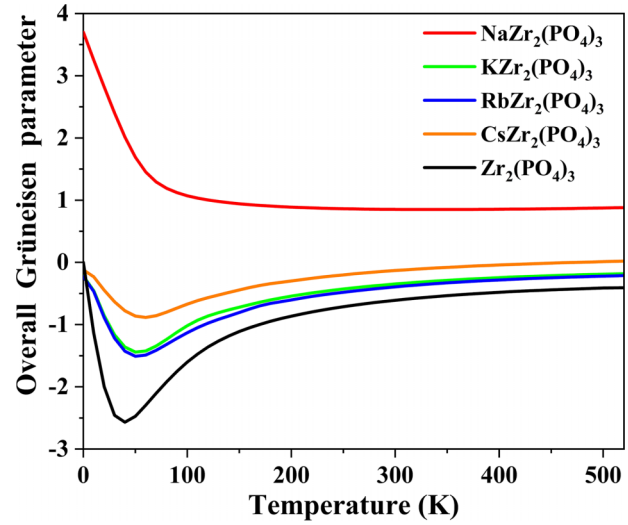

FIG. 8. Overall Grüneisen parameter $\bar{\gamma}$ calculated in $AZr_2(PO_4)_3$ compounds (A = Na, K, Rb, Cs) and $Zr_2(PO_4)_3$ as a function of temperature.

of ZrO_6 and PO_4 polyhedra. The calculated Grüneisen parameters reveal that when the *A*-site alkali metal ion changed, the contribution of specific three phonon models [(1) the mode dominated by *A*-site alkali metal ions; (2) rotation modes of ZrO_6 octahedron and PO_4 tetrahedron; (3) acoustic phonon modes] to NTE followed the order $KZr_2(PO_4)_3 \approx RbZr_2(PO_4)_3 > CsZr_2(PO_4)_3 > NaZr_2(PO_4)_3$, resulting in $KZr_2(PO_4)_3$ and $RbZr_2(PO_4)_3$ exhibiting similar low NTE properties, $CsZr_2(PO_4)_3$ exhibiting very weak NTE properties, and $NaZr_2(PO_4)_3$ exhibiting low PTE properties. When the *A* atom is absent, the structure flexibility increases result in the number of phonon modes contributing to the NTE increasing and becoming more easily excited, promoting the occurrence of the NTE. These results help us to understand the regulation of thermal expansion in NZP-type materials.

ACKNOWLEDGMENTS

This work was supported by the National Natural Science Foundation of China (Grants No. 22071221, No. 21905252, and No. 11874328) and Natural Science Foundation of Henan Province (Grants No. 212300410086 and No. 222301420040). All calculations were supported by National Supercomputing Center in Zhengzhou.

The authors declare no competing financial interest.

[1] A. Sleight, Zero-expansion plan, Nature (London) **425**, 674 (2003).

[2] X. Jiang, M. S. Molokeev, P. Gong, Y. Yang, W. Wang, S. Wang, S. Wu, Y. Wang, R. Huang, L. Li, Y. Wu, X. Xing, and Z. Lin, Near-zero thermal expansion and high ultraviolet transparency in a borate crystal of $Zn_4B_6O_{13}$, Adv. Mater. **28**, 7936 (2016).

[3] Y. Liu, D. Mei, N. Wang, M. S. Molokeev, X. Jiang, and Z. Lin, Intrinsic isotropic near-zero thermal expansion in $Zn_4B_6O_{12}X$ (X = O, S, Se), ACS Appl. Mater. Interfaces **12**, 38435 (2020).

[4] Y. Gao, C. Wang, Q. Gao, J. Guo, M. Chao, Y. Jia, and E. Liang, Zero thermal expansion in $Ta_2Mo_2O_{11}$ by compensation effects, Inorg. Chem. **59**, 18427 (2020).

[5] L. Hu, F. Qin, A. Sanson, L.-F. Huang, Z. Pan, Q. Li, Q. Sun, L. Wang, F. Guo, U. Aydemir, Y. Ren, C. Sun, J. Deng, G. Aquilanti, J. M. Rondinelli, J. Chen, and X. Xing, Localized symmetry breaking for tuning thermal expansion in ScF_3 nanoscale frameworks, J. Am. Chem. Soc. **140**, 4477 (2018).

[6] J. Z. Tao and A. W. Sleight, Very low thermal expansion in TaO_2F, J. Solid State Chem. **173**, 45 (2003).

[7] C. P. Romao, F. A. Perras, U. Werner-Zwanziger, J. A. Lussier, K. J. Miller, C. M. Calahoo, J. W. Zwanziger, M. Bieringer, B. A. Marinkovic, D. L. Bryce, and M. A. White, Zero thermal expansion in $ZrMgMo_3O_{12}$: NMR crystallography reveals origins of thermoelastic properties, Chem. Mater. **27**, 2633 (2015).

[8] M. K. Gupta, B. Singh, R. Mittal, and S. L. Chaplot, Negative thermal expansion behavior in $MZrF_6$ (M = Ca, Mg, Sr) : Ab initio lattice dynamical studies, Phys. Rev. B **98**, 014301 (2018).

[9] S. Margadonna, K. Prassides, and A. N. Fitch, Zero thermal expansion in a prussian blue analogue, J. Am. Chem. Soc. **126**, 15390 (2004).

[10] J. Liu, H. E. Maynard-Casely, H. E. A. Brand, and N. Sharma, $Sc_{1.5}Al_{0.5}W_3O_{12}$ exhibits zero thermal expansion between 4 and 1400 K, Chem. Mater. **33**, 3823 (2021).

[11] T. A. Mary, J. S. O. Evans, T. Vogt, and A. W. Sleight, Negative thermal expansion from 0.3 to 1050 kelvin in ZrW_2O_8, Science **272**, 90 (1996).

[12] Q. Gao, S. Zhang, Y. Jiao, Y. Qiao, A. Sanson, Q. Sun, X. Shi, E. Liang, and J. Chen, A new isotropic negative thermal expansion material of $CaSnF_6$ with facile and low-cost synthesis, Nano Res. **16**, 5964 (2023).

[13] E. Liang, Q. Sun, H. Yuan, J. Wang, G. Zeng, and Q. Gao, Negative thermal expansion: Mechanisms and materials, Front. Phys. **16**, 53302 (2021).

[14] L. Ding, C. Wang, Y. Na, L. Chu, and J. Yan, Preparation and near zero thermal expansion property of $Mn_3Cu_{0.5}A_{0.5}N$ (A = Ni, Sn)/Cu composites, Scr. Mater. **65**, 687 (2011).

[15] X. Yang, J. Xu, H. Li, X. Cheng, and X. Yan, In situ synthesis of ZrO_2/ZrW_2O_8 composites with near-zero thermal expansion, J. Am. Ceram. Soc. **90**, 1953 (2007).

[16] L. Hu, J. Chen, J. Xu, N. Wang, F. Han, Y. Ren, Z. Pan, Y. Rong, R. Huang, J. Deng, L. Li, and X. Xing, Atomic linkage flexibility tuned isotropic negative, zero, and positive thermal expansion in $MZrF_6$ (M = Ca, Mn, Fe, Co, Ni, and Zn), J. Am. Chem. Soc. **138**, 14530 (2016).

[17] X. Zhen, Q. Gao, A. Sanson, L. Tan, Y. Jiao, J. Wang, Q. Sun, and E. Liang, Origin of near-zero thermal expansion in $A_2O(PO_4)_2$ oxides over an ultrawide temperature range, J. Phys. Chem. C **126**, 21871 (2022).

[18] R. Chen, Q. Gao, Y. Qiao, J. Guo, and E. Liang, Continuous tailoring thermal expansion from giant negative to positive in $Ni_2P_2O_7$-based materials, Scr. Mater. **214**, 114653 (2022).

[19] Q. Gao, N. Shi, Q. Sun, A. Sanson, R. Milazzo, A. Carnera, H. Zhu, S. H. Lapidus, Y. Ren, Q. Huang, J. Chen, and X. Xing, Low-frequency phonon driven negative thermal expansion in cubic $GaFe(CN)_6$ prussian blue analogues, Inorg. Chem. **57**, 10918 (2018).

[20] Q. Gao, X. Shi, A. Venier, A. Carnera, Q. Huang, H. Wu, J. Chen, A. Sanson, and E. Liang, Effect of H_2O molecules on thermal expansion of $TiCo(CN)_6$, Inorg. Chem. **59**, 14852 (2020).

[21] J. Chen, Q. Gao, A. Sanson, X. Jiang, Q. Huang, A. Carnera, C. G. Rodriguez, L. Olivi, L. Wang, L. Hu, K. Lin, Y. Ren, Z. Lin, C. Wang, L. Gu, J. Deng, J. P. Attfield, and X. Xing, Tunable thermal expansion in framework materials through redox intercalation, Nat. Commun. **8**, 14441 (2017).

[22] D. M. Bykov, R. J. M. Konings, and A. I. Orlova, High-temperature investigations of the rare earth NZP phosphates $R_{1/3}Zr_2(PO_4)_3$ (R = La, Nd, Eu, Lu) by drop calorimetry, J. Alloys Compd. **439**, 376 (2007).

[23] M. V. Sukhanov, V. I. Pet'kov, and D. V. Firsov, Sintering mechanism for high-density NZP ceramics, Inorg. Mater. **47**, 674 (2011).

[24] Z. Jian, Y.-S. Hu, X. Ji, and W. Chen, NASICON-structured materials for energy storage, Adv. Mater. **29**, 1601925 (2017).

[25] E. Asabina, V. Pet'kov, P. Mayorov, D. Lavrenov, I. Schelokov, and A. Kovalsky, Synthesis, structure and thermal expansion of

the phosphates $M_{0.5+x}M'_xZr_{2-x}(PO_4)_3$ (M, M′–metals in oxidation state +2), Pure Appl. Chem. **89**, 523 (2017).

[26] V. Pet'Kov and A. Orlova, Crystal-chemical approach to predicting the thermal expansion of compounds in the NZP family, Inorg. Mater. **39**, 1013 (2003).

[27] J. Alamo, Chemistry and properties of solids with the [NZP] skeleton, Solid State Ionics **63**, 547 (1993).

[28] T. Oota and I. Yamai, Thermal expansion behavior of $NaZr_2(PO_4)_3$ type compounds, J. Am. Ceram. Soc. **69**, 1 (1986).

[29] Y. Hu, Q. Shao, H. Zhao, M. Chao, Q. Gao, J. Guo, X. Ren, and E. Liang, Investigation of the thermal shrink mechanism, thermal conductivity and compressive resistance of $TaTiP_3O_{12}$ ceramics, Ceram. Int. **49**, 6401 (2023).

[30] D. A. Woodcock, P. Lightfoot, and R. I. Smith, Negative thermal expansion behaviour in the NZP phase NbTi $(PO_4)_3$, MRS Online Proceedings Library **547**, 191 (1998).

[31] A. I. Orlova, G. N. Kazantsev, and S. G. Samoilov, Ultralow thermal expansion in the Cs-Ln-Zr and M-Hf phosphates (Ln = Pr, Sm, Gd; M = Na, K, Rb, Cs), High Temp. High Press. **31**, 105 (1999).

[32] S. Limaye, D. K. Agrawal, and H. McKinstry, Synthesis and thermal expansion of $MZr_4P_6O_{24}$ (M = Mg, Ca, Sr, Ba), J. Am. Ceram. Soc. **70**, C-232 (1987).

[33] K. G. Kutty, R. Asuvathraman, and R. Sridharan, Thermal expansion studies on the sodium zirconium phosphate family of compounds $A_{1/2}M_2(PO_4)_3$: Effect of interstitial and framework cations, J. Mater. Sci. **33**, 4007 (1998).

[34] E. Breval and D. K. Agrawal, Thermal expansion characteristics of [NZP], $NaZr_2P_3O_{12}$-type materials: A review, British Ceramic Transaction **94**, 27 (1995).

[35] T. Ota and I. Yamai, Low-thermal-expansion KZr sub 2(PO sub 4) sub 3 ceramic, Yogyo Kyokaishi **95**, 531 (1987).

[36] G. Kresse and J. Furthmüller, Efficient iterative schemes for ab initio total-energy calculations using a plane-wave basis set, Phys. Rev. B **54**, 11169 (1996).

[37] J. P. Perdew, K. Burke, and M. Ernzerhof, Generalized gradient approximation made simple, Phys. Rev. Lett. **77**, 3865 (1996).

[38] H. J. Monkhorst and J. D. Pack, Special points for brillouin-zone integrations, Phys. Rev. B **13**, 5188 (1976).

[39] A. Togo and I. Tanaka, First principles phonon calculations in materials science, Scr. Mater. **108**, 1 (2015).

[40] G. Kresse, J. Furthmüller, and J. Hafner, Ab initio force constant approach to phonon dispersion relations of diamond and graphite, Europhys. Lett. **32**, 729 (1995).

[41] A. Togo, L. Chaput, I. Tanaka, and G. Hug, First-principles phonon calculations of thermal expansion in Ti_3SiC_2, Ti_3AlC_2, and Ti_3GeC_2, Phys. Rev. B **81**, 174301 (2010).

[42] O. Hellman, I. A. Abrikosov, and S. I. Simak, Lattice dynamics of anharmonic solids from first principles, Phys. Rev. B **84**, 180301(R) (2011).

[43] O. Hellman, P. Steneteg, I. A. Abrikosov, and S. I. Simak, Temperature dependent effective potential method for accurate free energy calculations of solids, Phys. Rev. B **87**, 104111 (2013).

[44] S. d' Ambrumenil, M. Zbiri, A. M. Chippindale, and S. J. Hibble, Phonon dynamics in the layered negative thermal expansion compounds $Cu_xNi_{2-x}(CN)_4$, Phys. Rev. B **100**, 094312 (2019).

[45] S. d'Ambrumenil, M. Zbiri, A. M. Chippindale, S. J. Hibble, E. Marelli, and A. C. Hannon, Lattice dynamics and negative thermal expansion in the framework compound ZnNi $(CN)_4$ with two-dimensional and three-dimensional local environments, Phys. Rev. B **99**, 024309 (2019).

[46] L. H. N. Rimmer, M. T. Dove, B. Winkler, D. J. Wilson, K. Refson, and A. L. Goodwin, Framework flexibility and the negative thermal expansion mechanism of copper(I) oxide Cu_2O, Phys. Rev. B **89**, 214115 (2014).

[47] M. T. Dove, Z. Wei, A. E. Phillips, D. A. Keen, and K. Refson, Which phonons contribute most to negative thermal expansion in ScF_3? APL Mater. **11**, 041130 (2023).

[48] M. Calleja, A. L. Goodwin, and M. T. Dove, Origin of the colossal positive and negative thermal expansion in $Ag_3[Co(CN)_6]$: An ab initio density functional theory study, J. Phys.: Condens. Matter **20**, 255226 (2008).

[49] L. H. N. Rimmer, M. T. Dove, A. L. Goodwin, and D. C. Palmer, Acoustic phonons and negative thermal expansion in MOF-5, Phys. Chem. Chem. Phys. **16**, 21144 (2014).

[50] P. Vinet, J. H. Rose, J. Ferrante, and J. R. Smith, Universal features of the equation of state of solids, J. Phys.: Condens. Matter **1**, 1941 (1989).

[51] M. T. Dove and H. Fang, Negative thermal expansion and associated anomalous physical properties: Review of the lattice dynamics theoretical foundation, Rep. Prog. Phys. **79**, 066503 (2016).

[52] L. O. Hagman, P. Kierkegaard, P. Karvonen, A. Virtanen, and J. Paasivirta, The crystal structure of $NaMe^{IV}_2(PO_4)_3$; Me^{IV} = Ge, Ti, Zr, Acta Chem. Scand. **22**, 1822 (1968).

[53] E. R. Gobechiya, Y. K. Kabalov, V. I. Pet'kov, and M. V. Sukhanov, Crystal structures of double cesium zirconium and barium zirconium orthophosphates, Crystallogr. Rep. **49**, 741 (2004).

[54] H. Miyazaki, I. Ushiroda, D. Itomura, T. Hirashita, N. Adachi, and T. Ota, Thermal expansion of $NaZr_2(PO_4)_3$ family ceramics in a low-temperature range, Jpn. J. Appl. Phys. **47**, 7262 (2008).

[55] K. Kamali, T. R. Ravindran, and C. Ravi, Comparative raman spectroscopic study of phase stability and anharmonic effects in $AZr_2(PO_4)_3$ (A = K, Rb and Cs), Spectrochim. Acta Part A **155**, 38 (2016).

[56] Z. Wei, X. Jiang, A. E. Phillips, Z. Lin, and M. T. Dove, Phonons and low thermal expansion in sodalite zinc borate $Zn_4B_6O_{12}$ (X = O, S, Se), Phys. Rev. B **104**, 174310 (2021).